

Numerical Modeling of Liquid–Liquid Mass Transfer and the Influence of Mixing in Gas-Stirred Ladles

QUYNH N. HOANG,¹ MARCO A. RAMÍREZ-ARGÁEZ,²
ALBERTO N. CONEJO,³ BART BLANPAIN,⁴ and ABHISHEK DUTTA^{1,4,5}

1.—Faculty of Engineering Technology, KU Leuven, Campus Groep T Leuven, Andreas Vesaliusstraat 13, 3000 Leuven, Belgium. 2.—Department of Metallurgic Chemical Engineering, School of Chemistry, National Autonomous University of Mexico (UNAM), Edificio “D” Circuito de los Institutos s/n, Cd. Universitaria, C.P. 04510 Mexico, D.F., Mexico. 3.—School of Metallurgical and Ecological Engineering, University of Science and Technology Beijing (USTB), 30 Xueyuan Road, Haidian District, Beijing 100083, People’s Republic of China. 4.—Department of Materials Engineering, KU Leuven, Kasteelpark Arenberg 44, bus 2450, 3001 Heverlee-Leuven, Belgium. 5.—e-mail: abhishek.dutta@kuleuven.be

Ladle refining plays a key role in the steelmaking process. During the refining, a bubbly gas stream is used for mixing and to enhance the rate of removal of impurities from the molten steel. A numerical model has been developed to understand mass transfer and mixing behavior in a three-phase gas-stirred ladle. A two-resistance approach was used for the liquid–liquid mass transfer, while the mass transfer coefficient was determined using the Small Eddy theory. The model was validated with experimental data, obtained from a water–oil physical model simulating an industrial ladle with a scale factor of 1/17, valid for axisymmetric gas injection. Three variables were included to study the mass transfer behavior, namely gas flow rate, Q , oil (slag) thickness, h , and oil (slag) viscosity, μ_o . The gas flow rate ranged from 2.85 L/min to 8.56 L/min to meet industrial operating conditions. It was found that: (1) the volumetric mass transfer coefficient (ka) increases when the gas flow rate (Q) increases; and (2) increasing slag (oil) thickness has a positive influence on mass transfer as it considerably increases the interfacial area and promotes turbulence at the interface. At this range of gas flow rate, the effect of slag (oil) viscosity is limited. A general correlation was established: $ka = 0.058Q^{0.459}h^{0.612}$. Mixing time was studied within the same flow rate range to observe its influence on the mass transfer. Mixing in the ladle is accomplished in a much shorter time than interphase mass transfer, specifically by two orders of magnitude, which indicates that mass transfer is the rate-limiting step.

INTRODUCTION

The secondary refining process is an integral part of modern steelmaking, as its main objective is conditioning the liquid steel to achieve a homogeneous composition, an accurate casting temperature, and a high level of cleanliness in the steel.¹ A ladle furnace serves as a reactor in which processes, such as re-heating, temperature and chemical homogenization, inclusion removal, deoxidation and desulfurization, are performed.² The slag layer on top of the liquid steel retains undesirable chemical species such as sulfides. The liquid steel is

agitated by injecting gas (Ar/N₂), i.e., through porous plugs located in the bottom of the ladle, which produces a movement of recirculation in the liquid steel causing homogenization of thermal and chemical gradients, acceleration of metal–slag reactions, removal of gaseous species and flotation/precipitation of non-metallic inclusions.³ As a key to obtaining low-sulfur steel, the efficiency and productivity of the desulfurization process largely depends on: (1) the consecutive kinetic steps which consist of two main processes, namely the chemical reactions at the liquid–liquid interface and the mass transfer of sulfur from the metal to the slag phase,

and (2) mixing within the slag and the metal phases. It has been reviewed previously^{4,5} that the reactions at high temperature are mostly controlled by mass transfer rather than by interfacial chemical reactions; this is also applicable to the desulfurization process in a ladle furnace. During the desulfurization of liquid steel, sulfur dissolved in the metal phase is transported to the metal–slag interface, reacts with CaO (or MnO) and is transferred into the bulk slag. The transportation processes at the liquid–liquid interface involve diffusion of the reactant species, chemical reactions and diffusion of the reaction products to the slag phase. In reviewing the transport mechanism of solute (sulfur) from one phase to another across an interface, several empirical turbulent mass transfer models have been proposed to define the mass transfer coefficient in one phase, such as film theory, penetration theory, surface renewal theory, and eddy theory. The mass transfer coefficient is a parameter in empirical expressions that defines the mass transfer flux of a species at the interface. A brief description of these turbulent mass transfer models can be found in “Liquid–Liquid Mass Transfer” section.

The effect of mixing phenomena on liquid–liquid mass transfer and concentration distribution has not been studied much in the past. There have been some experimental studies^{4,6,7} which investigated the effect of various parameters such as gas flow rate, gas injection position and slag viscosity on the mass transfer rate. Of these, a comprehensive study by Kim and Fruehan⁴ has been commonly accepted as establishing a reasonable correlation between mass transfer volumetric coefficient and gas flow rate under different flow conditions. Their experimental studies, although leading to useful empirical correlations, were not sufficient to gain a detailed understanding of the underlying phenomena on a mesoscale. Typically, a numerical study is a complementary tool to experimental observations because it allows the analysis of a considerable number of variables and the estimation of the field values at locations where it is difficult to obtain experimental measurements.⁸ However, it must be noted that, with a numerical approach, it is challenging to determine numerically the mass transfer coefficient and the actual metal–slag interfacial area.²

The multiphase (involving gas and metal) modeling of a ladle furnace is already complex. Introducing a slag phase into the multiphase model results in a three-phase model which is intricate and computationally expensive. Several authors^{9–12} have written detailed reviews of physical and mathematical modeling of the ladle in the last few decades. The fluid dynamics and rate phenomena involved in a ladle furnace have been investigated using the computational fluid dynamics (CFD) approach which makes it possible to understand fluid flow and mass transfer mechanism on a mesoscale level¹³ mainly using two approaches:

the Eulerian model and the volume of fluid (VOF) model. The Eulerian model has been used to study fluid dynamics^{14–17} as well as mass transfer,^{18,19} while the VOF model is more applicable for studies about the behavior of the metal–slag interface.^{20–22}

Since both mass transfer and mixing can be correlated with the turbulent nature of fluid flow in a steel ladle,^{2,23} they are often studied together. The mixing phenomenon is well-characterized by several experimental²⁴ and mathematical^{25–31} studies with or without the inclusion of a slag phase. However, an appropriate choice of a liquid–liquid mass transfer model in a CFD study is difficult to ascertain, and so only a few studies^{21,32,33} have been conducted on this topic. Singh et al.²¹ developed a three-phase CFD model to determine the metal–slag interfacial area using the VOF approach. Costa et al.³² investigated the importance of the sulfur partition coefficient and the thickness of the slag layer on the desulfurization rate, with an input of the mass transfer coefficient based on Incropera and Dewitt’s³⁴ empirical correlation. Recently, Cao et al.³³ introduced a full-scale, three-dimensional, transient CFD model using the VOF approach to study the desulfurisation behavior. They adopted a generalized Kolmogorov theory of isotropic turbulence to study mass transfer. However, their analysis did not explain the transportation of species caused by different eddy scales, and therefore did not provide any insight into the mass transfer mechanism. To the best of our knowledge, there have been no mathematical studies about the metal–slag mass transfer in which the mixing characteristics are detailed and linked to mass transfer behavior. The aim of this study is to investigate the effect of mixing phenomena on the mass transfer coefficient based on a mass transfer model³⁵ using CFD, as it is important to investigate the influence of gas flow rate on the ladle desulfurization process, which is crucial for process optimization and intensification. It should be noted that the metal–slag emulsification effect is not included in this study because the gas flow rate is quite low, from 2.85 L/min to 8 L/min, resulting in the low specific rate of stirring energy (0.016–0.046 W/kg), which is considered insufficient to cause emulsification.³⁶ The gas flow rate, in the range tested, is compatible with the previous physical experiments³⁷ simulating an industrial-sized ladle of 140 tons with a scale factor of 1/17. The gas flow rate in experimental tests was estimated based on dynamic similarity criteria and the operating conditions of an industrial ladle (i.e., gas flow rate 0.2–0.6 m³/min) (see Ref. 37 for more details).

LIQUID–LIQUID MASS TRANSFER

In general, for mass transfer between two fluids, there are two-phase boundary layers causing resistance to the overall mass transfer. The mole flux, J , at the two-phase boundary in a steady state is:

$$J = k_m(C_m - C_m^e) = k_s(C_s^e - C_s) \quad (1)$$

where *m* and *s* denote for metal and slag, respectively, *k* (m/s) is the local mass transfer coefficient, *C* (mol/m³) the bulk concentration, and *C*^e (mol/m³) the equilibrium concentration at the interface.

Due to high affinity of sulfur with the slag phase, the mass transfer rate of species, *I*, from metal to slag is usually re-written in term of the metal phase as:

$$\dot{m} = -\frac{dC_i}{dt} = k_m \alpha (C_i - C_i^e) \quad (2)$$

where \dot{m} [mol/(m³s)] is the mass transfer rate and α (1/m) the interfacial area concentration ($\alpha = A/V$, where *A*, m² is the interfacial area and *V*, m³ is the volume of the concerned liquid).

In steel–slag mass transfer, the mass transfer coefficient, *k_m* (called hereafter *k*) can be estimated based on physicochemical and fluid-dynamic parameters. Various turbulence models have been developed taking into account the continuous renewal of the interface layer between two fluids due to chaotic fluid motion adjacent to the metal–slag interface caused by turbulence. Firstly, the Penetration theory (or Higbie’s theory) assumes that the stagnant fluid elements are exposed at the interface for a short, fixed period of time (*t_e*) during which they remain static so that molecular diffusion takes place.^{2,38} Secondly, the surface renewal model considers that, in a turbulent medium, the residence time of elements at the interface is varied following a certain distribution function; the rate of replacement of the element *s* is thus introduced. These two models have a limitation, as *t_e* or *s* is not explicitly defined. Therefore, based on the surface renewal theory, the eddy models have been developed to establish the link between the mass transfer coefficient with easily accessible parameters.

Similarly to other turbulent models, the eddy theory assumes that the fluctuating turbulent velocities are the dominating velocities near the interface. The eddies consisting of turbulence forces (inertial, pressure or viscous coupling), flow towards the interface, are deflected by the interface, travel along the interface, and subsequently plunge back into the fluid domain. This motion is responsible for bringing fresh fluid to the interface layer where mass transfer can occur by molecular diffusion. There is a wide range of eddy length scales present in a turbulent field which superimpose in a similar motion. The large eddies contain a majority of turbulent kinetic energy and are unstable, hence break into small eddies until all their energy is dissipated by viscous flow.³⁹ The large eddy model proposed by Fortescue and Pearson⁴⁰ assumes that large eddies are dominant in the mass transfer because they contain most of the turbulent energy. In an attempt to quantify the relative contributions of different sized motions, Lamont and Scott³⁵

proposed the small eddy model, postulating that the eddies in the boundary are usually small in size and they superimpose on large eddies, hence are more important than large eddies. The small eddy model was chosen for the current study due to the ease of accessing two parameters namely the energy dissipation rate, ε , and liquid kinematic viscosity, ν . The advantage of this model is the order of magnitude agreement with different types of interface.³⁵ More specifically, the small eddy theory determines the mass transfer coefficient by resolving the convective–diffusion equation. By replacing the velocity scale with the turbulent kinetic energy dissipation rate, the mass transfer coefficient can be represented as a function of molecular diffusivity, *D*, (m²/s), energy dissipation rate, ε , (m²/s³) and kinematic viscosity, ν , (m²/s):^{38,41}

$$k = 0.4\sqrt{D}\left(\frac{\varepsilon}{\nu}\right)^{0.25} \quad (3)$$

NUMERICAL MODEL DEVELOPMENT

Assumption

In the present study, a few assumptions were made, as follows:

- The ladle shape is simplified as cylindrical with a centric gas injection at the bottom.
- The gas-stirred ladle is axisymmetric.
- Water, silicone oil and air are used to replicate steel, slag and inert gas, respectively. The use of water satisfies the kinematic similarity criterion and the metal–slag system behaves similarly to the water–oil system.
- The physical properties of water, air and oil are constant.
- The system only allows the air to escape from the free open surface.
- It is assumed that the bubbles have a spherical shape and constant radius.
- Thymol (2-isopropyl-5-methylphenol), mentioned hereafter as the solute, is used in the role of sulfur as thymol has an equilibrium partition between oil and water similar to that of sulfur between metal and slag.
- The solute is exchanged between the water and oil phases, thermodynamic equilibrium is instantly established at the interface and the rate of exchange is controlled by mass transfer.
- The system is isothermal at 25°C.
- The solute and water are considered a homogeneous solution throughout the domain of the initial aqueous phase.

Governing Equations

The fluid flow phenomena and the liquid–liquid mass transfer are simulated using the Euler–Euler approach solving the Reynolds’ averaged Navier–

Stokes equations. As flows involve species transfer, additional species conservation equations are included. Since the ladle geometry is axisymmetric, the governing equations are resolved in two dimensions. The physical properties of all three phases can be found in Table I. The continuity equation is established according to the mass conservation principle. The continuity equation for phase q is:

$$\frac{\partial}{\partial t}(\alpha_q \rho_q) + \nabla \cdot (\alpha_q \rho_q \vec{u}_q) = 0, \quad (4)$$

where \vec{u}_q (m/s) is the velocity of phase q , and ρ_q (kg/m³) is the density. The different phases are treated as interpenetrating continua and the volume of one phase cannot be occupied by the other phases. The volume of phase q is defined by:

$$V_q = \int \alpha_q dV, \quad (5)$$

where α_q is the volume fraction of the phase q , n is the number of phases, and $\sum_{q=1}^n \alpha_q = 1$

The momentum equation for phase q is:

$$\begin{aligned} \frac{\partial}{\partial t}(\alpha_q \rho_q \vec{u}_q) + \nabla \cdot (\alpha_q \rho_q \vec{u}_q \vec{u}_q) = & -\alpha_q \nabla p + \nabla \cdot \bar{\tau}_q \\ & + \alpha_q \rho_q \vec{g} + \sum_{p=1}^n \vec{R}_{pq} + \sum \vec{F}, \end{aligned} \quad (6)$$

where $\bar{\tau}_q$ [kg/(ms²)] is the stress tensor of phase, q , estimated by the k - ε turbulence equations,⁴⁰ \vec{g} (m/s²) is the gravity constant, p (Pa) is the pressure, \vec{F} (kg/m² s²) represents different forces acting on the fluid elements (e.g., external body force, turbulent dispersion force), and \vec{R}_{pq} (kg/m² s²) is the interaction force between phases. The turbulent kinetic energy, k , (J/kg) and its dissipation rate, ε , (m²/s³) of phase q are obtained from the following transport equations:

$$\begin{aligned} \frac{\partial}{\partial t}(\alpha_p \rho_q k_q) + \nabla \cdot (\alpha_p \rho_q \vec{u}_q k_q) = & \nabla \\ & \cdot \left[\alpha_q \left(\mu_q + \frac{\mu_{t,q}}{\sigma_k} \right) \nabla k_q \right] + \alpha_p G_{k,q} + \alpha_p G_{b,q} - \alpha_p \rho_q \varepsilon_q \end{aligned} \quad (7)$$

Table I. Geometry set-up and material properties

Parameter	Initial	Unit	Value
Water height	H	m	0.1648
Silicon oil thickness	h	m	0.0066
Ladle diameter	D	m	0.189
Air flow rate	Q_m	L/m	2.85
Air density	ρ_A	kg/m ³	1.225
Air viscosity	μ_A	kg/ms	1.79E-5
Water density	ρ_W	kg/m ³	998.2
Water viscosity	μ_W	kg/ms	0.001003
Silicone oil density	ρ_O	kg/m ³	800
Silicone oil viscosity	μ_O	kg/ms	0.0832

$$\begin{aligned} \frac{\partial}{\partial t}(\alpha_p \rho_q \varepsilon_q) + \nabla \cdot (\alpha_p \rho_q \vec{u}_q \varepsilon_q) = & \nabla \cdot \left[\alpha_q \left(\mu_q + \frac{\mu_{t,q}}{\sigma_\varepsilon} \right) \nabla \varepsilon_q \right] \\ & + \alpha_q C_{1\varepsilon} \frac{\varepsilon_q}{k_q} (G_k + C_{3\varepsilon} G_b) - \alpha_q C_{2\varepsilon} \rho_q \frac{\varepsilon_q^2}{k_q}, \end{aligned} \quad (8)$$

where G_k (kg/ms³) and G_b (kg/ms³) are the generation of turbulence kinetic energy due to the mean velocity gradients and buoyancy, $C_{1\varepsilon}, C_{2\varepsilon}, C_{3\varepsilon}$ are constants, $\sigma_k, \sigma_\varepsilon$ are Prandtl numbers for k and ε with constant values, μ (Pa s) is the dynamic viscosity, and μ_t (Pa s) is the eddy viscosity.

Since the study of mixing time requires the tracking of fluid elements, the transport equation of a tracer is involved. The local mass fraction of tracer, Y_i , is estimated by using the following equation, considering the net rate of production and creation of species is zero.⁴²

$$\frac{\partial}{\partial t}(\rho Y_i) + \nabla \cdot (\rho \vec{u} Y_i) = \nabla \cdot \left(\frac{\mu_t}{Sc_t} (\nabla Y_i) \right), \quad (9)$$

where Sc_t is the turbulent Schmidt number.

Mass Transfer Model

The interphase species mass transfer model⁴² was chosen for this study, given that it deals with mass transfer occurring across the interface, which is physically reasonable for the steel–slag interaction described in “Liquid–Liquid Mass Transfer” section. The phase species transport equations are solved along with the phase mass, momentum and energy equations. The transport equation for Y_q^i , the local mass fraction of species i in phase q , without reaction, is:

$$\begin{aligned} \frac{\partial (\alpha_q \rho_q Y_q^i)}{\partial t} + \nabla \cdot (\alpha_q \rho_q \vec{u}_q Y_q^i) = & -\nabla \cdot (\alpha_q \vec{J}_q) \\ & + \sum_{p=1}^n (\dot{m}_{p^i q^i} - \dot{m}_{q^i p^i}) \end{aligned} \quad (10)$$

where \vec{J}_q (kg/m² s) is the diffusion flux of species, \dot{m} (kg/m³ s) is the mass transfer rate (i.e., the source term):

$$\dot{m}_{p^i q^i} = k_{pq} \alpha_i (\rho_{q,e}^i - \rho_q^i), \quad (11)$$

where k_{pq} and k_{qp} (m/s) are the volumetric mass transfer coefficients between the p and q phases, input by user-defined function code based on Eq. 3; α_i is the interfacial area concentration, ρ_q^i the mass concentration of species i in phase q , and $\rho_{q,e}^i$ the equilibrium mass concentration of species i in phase q .

Initial and Boundary Conditions

A two-dimensional model of a ladle was built using ANSYS Design Modeler 17.0. The cylindrical ladle has a diameter of 0.189 m and a height of 0.2248 m, similar to that of the envisaged physical model.³⁷ Since the ladle is axisymmetric, only the X – Y plane was considered. At the symmetry axis, fluxes for all the transported quantities are zero. A nozzle with a diameter of 0.01 m was specified at the center of the bottom where the air inlet boundary condition was set. At the bottom and lateral ladle impermeable walls, non-slip conditions were applied. In addition, the standard wall function was chosen to treat the flow field at the wall sublayer between the laminar region near the wall and the turbulent core in the ladle. Atmospheric pressure was considered at the free open boundary.

Initially, all phases are static and are accommodated according to their densities. The initial conditions for the study of fluid dynamics and turbulence involve three different layered structures: water is present at the bottom (height = 0.164 m), followed by a layer of oil on top of water (thickness = 0.0065 m) and finally an air layer on top of the oil. The velocity of all components and turbulent parameters begin with zero values throughout the domain. Although an industrial ladle furnace is not isothermal, thermal gradients during operation are low inside, since it is well stirred. This has helped to simplify the model by assuming isothermal conditions as heat transfer inside the bath is not within the scope of this study. Mass transfer was calculated once the water–oil–air system has established a quasi-steady flow pattern in fluid dynamics, i.e., recirculation and velocities in the liquid remain constant over time. The initial condition for this calculation began with a homogeneous solution between the solute and water phase at a concentration of 125 ppm thymol and with zero initial concentration of solute in the oil phase.

Computational Requirement

Structured meshing was carried out using ANSYS Workbench Mesh Generation 17.0. Fine meshing at the water–oil and oil–gas interfaces can resolve the surface deformation accurately and avoid numerical diffusion. A grid dependence test, using the grid convergence index (GCI) based on Roache,⁴³ was carried out to identify the optimal mesh for accuracy and computation time. The study was performed with three different set of grids namely, coarse mesh (A), finer mesh (B), and finest mesh (C) with a refinement factor of 1.5 which contain 7524, 16,830, and 37,995 mesh cells respectively. Three simulations were run transiently having a configuration of Intel® Core™ i5-4300U with a clock speed of 1.9 GHz and 8 GB of RAM. It took 4.92, 6.54 and 11.58 s of computer time for each time step for cases A, B and C respectively. The

time-averaged water velocity near the water–oil interface (i.e., along the X axis at a ladle height of 0.12 mm) was examined. It was estimated that the average local order of accuracy is 3, and the average GCI is 16% with a general range from 0% to 25% and four points at 30–100%, giving the maximum uncertainty of 0.02 m/s. This variation can be explained by the unsteadiness and the complexity of the flow around the interface. In general, results from meshes B and C have a similar accuracy while the computer time needed for mesh C is two times higher as compared to mesh B. Therefore, mesh B was considered for the simulations.

The numerical solution of the study was developed transiently using a time step of 10^{-4} s, 20 iterations per time step. Each simulation took 20 s of real time to reach a quasi-steady state. Simulations were run in VSC HPC cluster, thinking node: 16-core Ivy Bridge Xeon E5-2680v2 CPU with a clock speed of 2.8 GHz and 64 GB RAM. It took 50 h of computer time to reach this state, using 4 processors in parallel.

Experimental Study

An air–water–oil physical model³⁷ was constructed with the scaling factor of 1/17 representing an industrial-size ladle of 250 tons. Air was injected through a 0.01-m nozzle located at the bottom of the ladle. To study the flow field, Ramírez-Argáez and González-Rivera³⁷ used particle image velocimetry as a fluid visualization technique to obtain real-time velocity maps in a region of interest in the fluid. For a detailed explanation of the validation setup, the interested reader is suggested to read the cited reference. In the mass transfer experiments, thymol (2-isopropyl-5-methylphenol) was used in the role of sulfur to investigate the behavior of the solute in the ladle, and silicon oil was used in the role of slag.

RESULTS AND DISCUSSION

Model Validation

Figure 1 shows the mass transfer resemblance behavior between the numerical and experimental data. Compared to the experimental data, the error of the numerical prediction lies within a band of $\pm 5\%$ (shown in red). As seen in the figure, the mass transfer process is rather slow. In the beginning, it takes 15 min to remove about 20% the amount of thymol from the water phase, as the oil phase has a strong affinity to thymol. After 90 min, once the thymol concentration in the two phases approaches an equilibrium state, it takes about 30 min to remove 7–8% of the thymol. The mass transfer behavior follows the exponential rule, explained by a first-order kinetic mechanism well-established by several researchers.^{2,4} The notable agreement with the experimental data proves the applicability of the small eddy theory. This theory assumes that small eddies at the water–

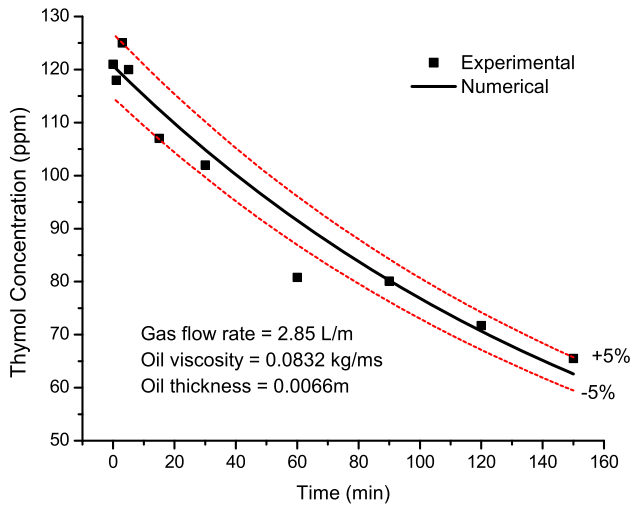


Fig. 1. Liquid-liquid mass transfer behavior (experimental and predicted).

oil interface are of utmost importance in the transport process. Small eddies are formed from the unstable large eddies that break up by the dissipation of turbulent kinetic energy. These smaller eddies undergo a similar break-up process and transfer their energy to yet smaller eddies. A high rate of turbulence dissipation indicates the notable presence of small eddies at the top edge of the ladle. According to the small eddy theory, these small eddies superimpose the flow near the interface and are therefore mostly responsible for transportation of species (i.e., thymol) at the interface.

Sensitivity Analysis

Effect of Gas Flow Rate

As mentioned earlier, the mass transfer in the ladle is closely correlated to the motion of the main fluid which, in this study, is liquid water. The flow is mainly caused by the forced convection due to gas stirring; hence, the impact of gas flow rate on the liquid-liquid mass transfer has been studied. The water flow pattern, which was obtained from the CFD simulations, shows a trend in agreement with the literature summarized by Ghosh.² In the middle, the two-phase region consisting of gas bubbles and liquid water (commonly referred to as the plume) is formed; the plume moves upward and pushes the oil to the periphery of the ladle. At the free surface, the raised liquid drags the bubbles, deforms the air-water interface, and creates an area called the “open eye”. Because of turbulence, the fluid moves rapidly from the center to the side of the ladle and slows along the wall, then returns to the plume to complete a recirculation loop. Figure 2 illustrates the relationship between the mass transfer parameter, ka , and the gas flow rate, Q , ranging from 2.85 L/m to 8.56 L/m. It is seen that ka increases linearly with $Q^{0.55}$ (R -squared = 97.9%).

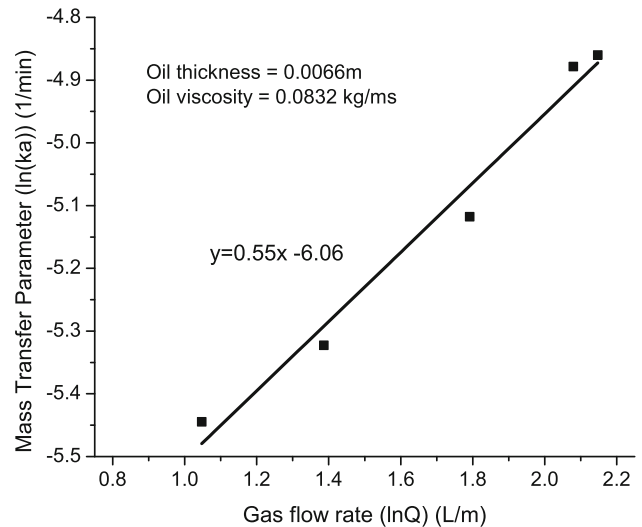


Fig. 2. Effect of gas flow rate on mass transfer parameter, ka .

To understand the phenomenon behind the evolution of the mass transfer parameter with respect to the gas flow rate, several factors, including oil volume fraction, water velocity, eddy viscosity and turbulent eddy dissipation rate, were investigated. Figure 3 indicates the volume fraction of oil at different gas flow rates. The water-oil interface is located mainly in the periphery of the ladle where the oil volume fraction is less than 1, meaning that the remaining part is occupied by the water volume fraction. The figure shows a relatively minor difference between the four cases, meaning that, at low gas flow rates, the impact of gas flow rate on the total interfacial area seems insignificant. From Fig. 4, it can be observed that the water velocity near the interface is larger at higher gas flow rates. This is because a stronger agitation, caused by a higher gas flow rate, promotes recirculation and improves mass transfer. The turbulence near the water-oil interface is also improved, as the water eddy viscosity and the turbulent eddy dissipation rate are generally more intense at higher gas flow rates. To summarize, although the gas flow rate does not have much influence on the interfacial area, it clearly affects eddy diffusion and therefore controls mass transfer in this specific gas flow rate regime. This result shows a good agreement with several studies. Hirasawa et al.⁴⁴ established a correlation between the mass transfer coefficient, k , and the gas flow rate in a $\text{Li}_2\text{O-SiO}_2\text{-Al}_2\text{O}_3$ slag-molten Cu reaction system for Si oxidation. They found that k varies with Q at a different exponent of dependency, depending on the range of gas flow rate. In particular, at a specific low gas flow rate, k is proportional to the square root of Q . Further attempts were made to verify the relationship between k and $Q^{0.5}$, such as by Staples and Robertson,⁴⁵ who performed mercury-water physical experiments, and by Taniguchi et al.,⁴⁶ who

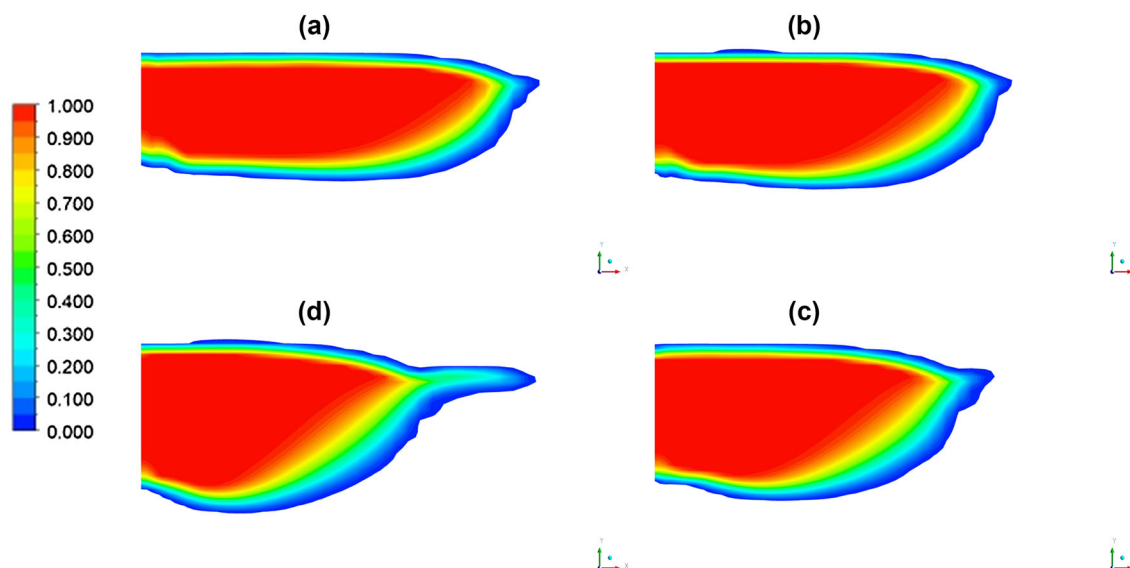


Fig. 3. Contours of oil volume fraction at different gas flow rates: (a) $Q = 2.85$ L/min, (b) $Q = 4$ L/min, (c) $Q = 6$ L/min, and (d) $Q = 8$ L/min.

measured the rate of CO_2 absorption at the free surface of a water bath. Likewise, previous experimental investigations^{4,47–49} have also identified a direct relationship between the gas flow rate and the volumetric mass transfer coefficient. The exponent on the gas flow rate is an indication of the intensity that this variable affects mass transfer. However, the exponent values reported in these experimental studies have a large discrepancy, ranging from 0.4 to 1.4. This can be explained by a complex emulsification effect inside the ladle, which is specific to each multiphase system. It is well known⁵⁰ that emulsification is enhanced in those systems, with a low density ratio between the two liquid phases. In cases where emulsification occurs, mass transfer is largely increased because of a substantial rise in interfacial area. The exponent cannot therefore be compared directly if the systems are different. It is necessary to clarify that the present model is only attributed to a particular water–oil system investigated at low gas flow rates and not suited to predict emulsification.

Effect of Slag Thickness

Figure 5 shows the relationship between the oil (i.e., slag) thickness and the mass transfer parameter, ka . It can be seen that an increase in slag thickness causes a significant increase in mass transfer rate. There are several explanations for this trend. The most general explanation is that the slag eye area decreases as the slag thickness increases, promoting a higher interfacial area.^{21,44} In addition to this, the mass fraction of sulfur (i.e., thymol) decreases when the volume of the slag increases; the driving force for mass transfer from the water to the slag phase is thus increased.²⁸ The slag volume fraction contours obtained from the

numerical model fit very well with this explanation, as the interfacial area increases with the slag thickness. Regarding turbulence, there are, however, some conflicts in explaining the impact of slag thickness. Singh et al.²¹ and Hirasawa et al.⁴⁴ stated that the slag thickness has little or almost no influence on k , meaning that only fluid flow in the metal phase is considered to influence the metal-side mass transfer. In contrast, Kim and Fruehan⁴ and Cao et al.³³ found that a high volume of slag promotes a stronger circulation inside the slag layer. With the numerical approach, it is possible to investigate this phenomenon in greater detail. Based on the water eddy viscosity and water eddy dissipation rate fields obtained from the CFD models, it confirms that the turbulence tends to be stronger because of the presence of more slag, resulting in a better transportation of species.

Effect of Slag Viscosity

Figure 6 indicates that the oil (i.e., slag) viscosity has a negligible effect on the volumetric mass transfer coefficient, ka , taking into account that there is a small tendency that the volumetric mass transfer coefficient decreases as the slag viscosity increases. At low gas flow rates, with a two-fold increase in slag viscosity from 40 cP to 83 cP (0.04 kg/ms to 0.083 kg/ms) there is a decrease of less than 5% in the volumetric mass transfer coefficient. At higher gas flow rates, there are no differences in the volumetric mass transfer coefficient as the gas flow rate increases. This behavior is because the main forces that affect mixing phenomena are inertial and gravitational, while the viscous forces play a minor role. Similar observations were also reported by Kim and Fruehan⁴ and Patil et al.⁵¹ The latter measured mixing time using four

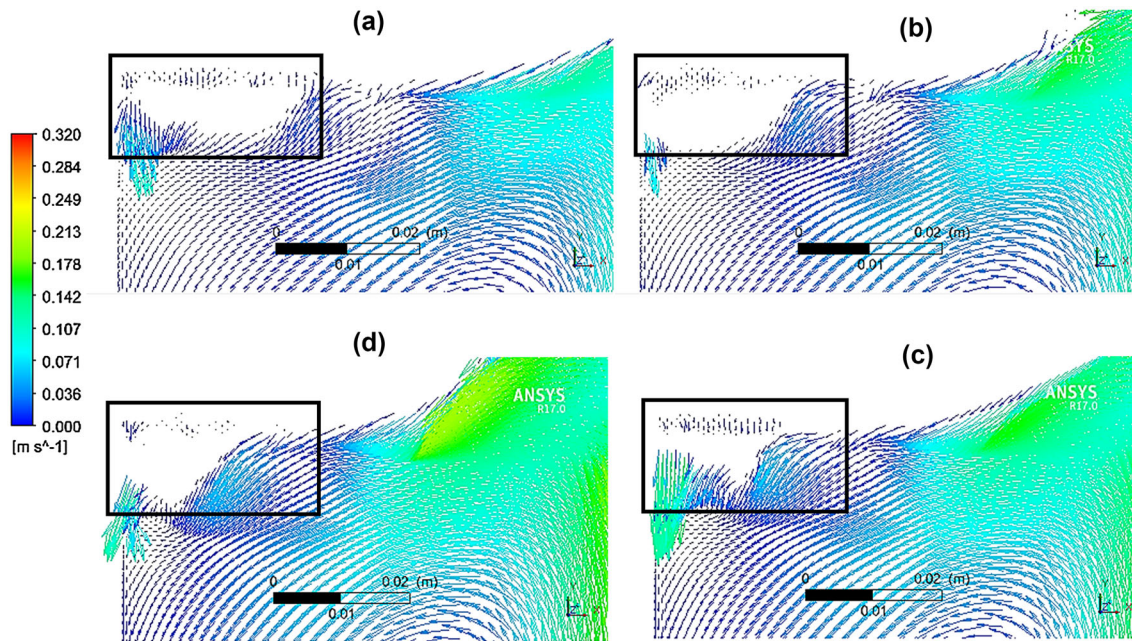


Fig. 4. Flow field of water at different gas flow rates near the water–oil interface (indicated in a box): (a) $Q = 2.85$ L/min, (b) $Q = 4$ L/min, (c) $Q = 6$ L/min, and (d) $Q = 8$ L/min.

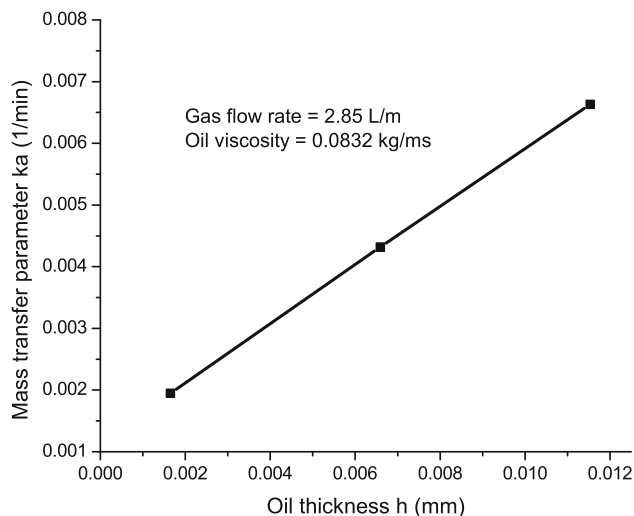


Fig. 5. Effect of slag thickness on mass transfer parameter at $Q = 2.85$ L/min.

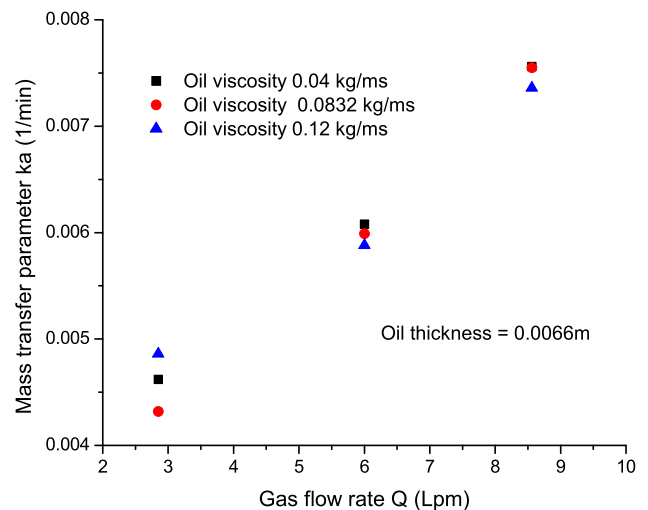


Fig. 6. Effect of slag viscosity on mass transfer parameter at different gas flow rates.

different types of oils with different viscosities. The final relationship, derived from dimensional analysis, reported an exponent of 0.016 on the term associated with the slag viscosity, in contrast to values from 0.3 to 1 for other terms involving the gas flow rate, height of liquid steel or slag thickness.

Mass Transfer Correlation

The gas flow rate (Q , L/min) and the oil thickness (h , m) was correlated with the liquid–liquid mass transfer parameter (ka , 1/min) by using multiple regression analysis. The results of fitting a multiple

linear regression model (with R -squared of 98%) describe the relationship between ka and two independent variables, Q and h :

$$ka = 0.0586Q^{0.459}h^{0.612} \quad (12)$$

This equation is valid for a range of gas flow rates from 2.85 L/min to 8.56 L/min and of oil thickness from 1.65 mm to 11.54 mm. Based on this, the relationship between volumetric mass transfer parameter and gas flow rate is corrected to $ka \sim Q^{0.46}$.

Mixing Time

The efficiency of a physical–chemical process depends largely on the mixing degree. To understand the transport phenomena in a gas-stirred system, the mixing behavior needs to be investigated. Traditionally, the mixing efficiency of a specific ladle is simply qualified as the mixing time. By definition, mixing time is the time taken to homogenize the liquid contents of the fluid domain after a step change in composition.²⁶ Physically, measuring all the local concentrations of a tracer is infeasible, and there always exist some dead points where instantaneous concentration never reaches the average homogenous value of the fluid domain. Therefore, a set of monitoring points have been chosen and a specific mixing time measured for each point; the mixing time t_{mix} is then defined to be an average of these measurements. At a gas flow rate of 2.85 L/min, the mixing time is 8.3 s, considering the degree of mixing of 0.95. Figure 7 shows the relationship between mixing time and gas flow rate described by the following expression:

$$t_{\text{mix}} = 12.55Q^{-0.412}, \quad (13)$$

where t_{mix} is in s and Q is in L/min. The result from this study is in accordance with well-established investigations. Without the presence of the slag phase, Asai et al.²⁴ and Mazumdar⁵² established the relationship for Froude-dominated flows: $t_{\text{mix}} \sim Q^{-0.333}$. The presence of the slag layer causes an increase in the mixing time due to a loss of energy and slowing down of recirculatory flow,^{2,52–54} thus $t_{\text{mix}} \sim Q^{-0.412}$ as compared to $t_{\text{mix}} \sim Q^{-0.333}$. Thus Eq. 13 has the higher exponent and therefore the higher dependency on the gas flow rate, Q . A similar finding was reported by Kim and Fruehan⁴ when $n = -0.32$ without a slag layer and $n = -0.43$ with slag layer.

Mass Transfer and Mixing Time

In general, liquid–liquid mass transfer and mixing are both treated as first-order reversible processes. Mixing time is defined for homogenization, while mass transfer is defined in terms of conversion. From the literature, mixing time (95% homogenization) and 95% conversion time for mass transfer-controlled reactions are in the same overall range.² However, in this study, at a gas flow rate of 2.85 L/min, mixing time is approximately 5–8 s, while 95% conversion requires 140 min, equivalent to 8400 s. In other words, mixing inside the ladle is accomplished at a much shorter time, but the full removal of impurities requires a much longer time, specifically by two orders of magnitude, which proves that mass transfer is the rate-limiting step in the process, as was also noted by Kim and Fruehan.⁴ When the gas flow rate increases, mixing occurs more quickly and the mass transfer rate increases; the process is therefore optimized.

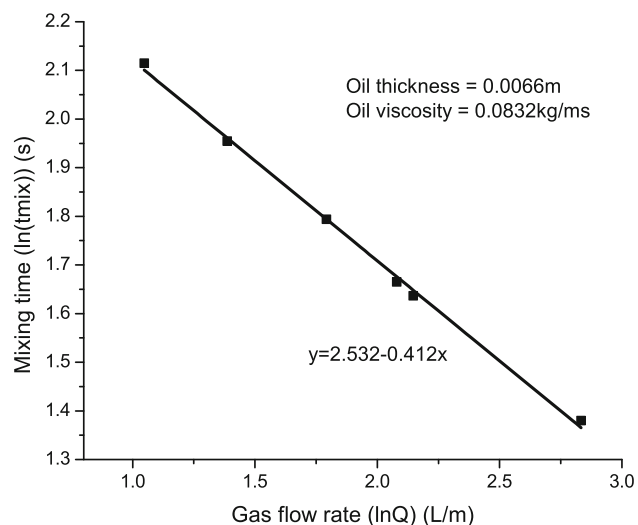


Fig. 7. Logarithmic relationship between mixing time and gas flow rate.

CONCLUSION

A comprehensive numerical model has been developed to study the liquid–liquid mass transfer in gas-stirred ladles under low gas flow rate conditions. The two-resistance approach has been used to compute the mass transfer behavior based on the small eddy theory. A good agreement is obtained between the numerical and the experimental results. Both the mass transfer parameter and the mixing time are found to be directly dependent on the gas flow rate. The mass transfer parameter, ka , is proportional to $Q^{0.46}$ while the mixing time is inversely proportional to $Q^{0.412}$. In a low gas flow rate regime (i.e., from 2.85 L/m to 8 L/m), when the gas flow rate increases, the mixing process is enhanced and mass transfer occurs more quickly. Based on the difference in the magnitude of the time needed for mixing and 95% conversion for mass transfer, it can be concluded that the desulfurization rate in a ladle is mass transfer-controlled. The mass transfer parameter was correlated with the gas flow rate, the oil thickness and the oil viscosity. The oil thickness is found to positively affect the mass transfer rate, while the oil viscosity does not influence the mass transfer process. When the oil thickness increases, mass transfer occurs more quickly due to a substantial increase in the interfacial area, a stronger turbulence and a higher driving force. Based on these observations, a mathematical correlation involving air (gas) flow rate, oil (slag) thickness was established.

REFERENCES

1. S. Du, *Improving Process Design in Steelmaking, Fundamentals of Metallurgy* (Cambridge: Woodhead Publishing Limited, 2005), pp. 369–398.
2. A. Ghosh, *Secondary Steel Making: Principles and Applications* (Boca Raton: CRC Press LLC, 2001).

3. G.J.W. Kors and P.C. Glaws, *Ladle Refining and Vacuum Degassing, the Making, Shaping and Treating of Steel* (Pittsburgh: The AISE Steel Foundation, 1998), pp. 661–713.
4. S. Kim and R.J. Fruehan, *Metall. Trans. B* 18B, 381–390 (1987).
5. K. Mori, *Trans. ISIJ* 28, 246–261 (1988).
6. K. Ogawa and T. Onoue, *ISIJ Int.* 29, 148–153 (1989).
7. M. Martín, M. Rendueles, and M. Díaz, *Chem. Eng. Res. Des.* 83, 1076–1084 (2005).
8. A. Dutta, R.P. Ekampure, G.J. Heynderickx, A. de Broqueville, and G.B. Marin, *Chem. Eng. Sci.* 65, 1678–1693 (2010).
9. D. Mazumdar and R.I.L. Guthrie, *ISIJ Int.* 35, 1–20 (1995).
10. P.G. Jönsson and L.T.I. Jonsson, *ISIJ Int.* 41, 1289–1302 (2001).
11. D. Mazumdar and J.W. Evans, *ISIJ Int.* 44, 447–461 (2004).
12. G.A. Irons, A. Senguttuvan, and K. Krishnapisharody, *ISIJ Int.* 55, 1–6 (2015).
13. Y. Zang, X. Zang, B. Xu, W. Cai, and F. Wang, *Can. J. Chem. Eng.* 93, 2307–2314 (2015).
14. J.L. Xia, T. Ahokainen, and L. Holappa, *Scand. J. Metall.* 30, 69–76 (2001).
15. J.L. Xia and T. Ahokainen, *Metall. Mater. Trans. B* 32, 733–741 (2001).
16. H. Türkoğlu and B. Farouk, *Metall. Trans. B* 21, 771–781 (1990).
17. W. Lou and M. Zhu, *Metall. Mater. Trans. B* 44, 1251–1263 (2013).
18. G. Venturini and M.B. Goldschmit, *Metall. Mater. Trans. B* 38, 461–475 (2007).
19. M. Al-Harbi, H.V. Atkinson, and S. Gao, *Proceedings of the XIth MCWASP* (Opio, 2006).
20. B. Li, H. Yin, C.Q. Zhou, and F. Tsukihashi, *ISIJ In.* 48, 1704–1711 (2008).
21. U. Singh, R. Anapagaddi, S. Mangal, K.A. Padmanabhan, and A.K. Singh, *Metall. Mater. Trans. B* 47B, 1804–1816 (2016).
22. S. Lin, H. Chen, and D. Xie, *Asia-Pacific Energy Equipment Engineering Research Conference* (2015), pp. 310–313.
23. K. Nakanishi, J. Szekeley, and C.W. Chang, *Ironmaking Steelmaking* 2, 115–124 (1975).
24. S. Asai, T. Okamoto, J. He, and I. Muchi, *Trans. ISIJ* 23, 43–50 (1983).
25. M. Zhu, T. Inomoto, I. Sawada, and T. Hsiao, *ISIJ Int.* 35, 472–479 (1995).
26. S.W.P. Cloete, J.J. Eksten, and S.M. Bradshaw, *Miner. Eng.* 46–47, 16–24 (2013).
27. S. Ganguly and S. Chakraborty, *Ironmaking Steelmaking* 35, 524–530 (2008).
28. W. Lao and M. Zhu, *ISIJ Int.* 54, 9–18 (2014).
29. L. Li, Z. Liu, B. Li, H. Matsuura, and F. Tsukihashi, *ISIJ Int.* 55, 1337–1346 (2015).
30. M.A. Ramirez-Argaez, A. Conejo, and A. Amaro-Villeda, *ISIJ Int.* 54, 1–8 (2014).
31. A. Chaendera and R.H. Eric, *Effect of Slag Phase on Mixing and Mass Transfer in a Model Creusot Loire Uddeholm (CLU) Converter* (The Mineral, Metals & Materials Society, 2017), pp. 45–61.
32. L.T. Costa and R.P. Tavares, *Mass Transfer-Advancement in Process Modelling*, ed. by M. Solecki (InTech, New York, 2015), pp. 149–167.
33. Q. Cao, A. Pitts, and L. Nastac, *Ironmaking Steelmaking* 45, 280–287 (2018).
34. F.P. Incropera and D.P. DeWitt, *Introduction to Heat Transfer* (New York: Wiley, 2002).
35. J.C. Lamont and D.S. Scott, *AIChE J.* 16, 513–519 (1970).
36. V. Sahajwalla, J.K. Brimacombe, and M.E. Salcudean, *Steelmaking Conf., Proceedings ISS*, Vol. 72 (1989), pp. 497–501.
37. M. Ramírez-Argáez and C. González-Rivera, *The 3rd Pan American Materials Congress* (2017).
38. L. Dong, S.T. Johansen, and T.A. Engh, *Can. J. Metall. Mater. Sci.* 31, 299–307 (1992).
39. P.H. Calderbank and M.B. Moo-Young, *Chem. Eng. Sci.* 16, 39–54 (1961).
40. G.E. Fortescue and J.R.A. Pearson, *Chem. Eng. Sci.* 22, 1163–1176 (1967).
41. L.P. Hung, C.S. Garbe, and W. Tsai, *The 6th International Symposium on Gas Transfer at Water Surfaces* (2010), pp. 17–21.
42. ANSYS Fluent Theory Guide 17.0, ANSYS Inc, 2016.
43. P.J. Roache, *ASME J. Fluids Eng.* 71, 405–413 (1994).
44. M. Hirasawa, K. Mori, M. Sano, A. Hatanaka, Y. Shimatani, and Y. Okazaki, *Trans. ISIJ* 27, 277–282 (1987).
45. D.G.C. Robertson and B.B. Staples, *Process Engineering of Pyrometallurgy* (Institution of Mining and Metallurgy, London, 1974), pp. 51–59.
46. S. Taniguchi, S. Kawaguchi, and A. Kikuchi, *Appl. Math. Model.* 26, 249–262 (2002).
47. Y. Ohga, S. Taniguchi, and J. Kikuchi, *Tetsu-to-Hagane* 71, S897 (1985).
48. M. Hirasawa, K. Mori, M. Sano, Y. Shimada, and Y. Okazaki, *Tetsu-to-Hagane* 71, S898 (1985).
49. S. Endo and M. Hasegawa, *Tetsu-to-Hagane* 71, S899 (1985).
50. S. Joo and R.I.L. Guthrie, *Metall. Trans. B* 23, 765–778 (1992).
51. S.P. Patil, D. Satish, M. Peranandhanathan, and D. Mazumdar, *ISIJ Int.* 50, 1117–1124 (2010).
52. D. Mazumdar, Fluid flow, Particle motion and mixing in ladle metallurgy operations, PhD Thesis, McGill University, Montreal, 1985.
53. Q. Ying, L. Yun, and L. Liu, *Scaninject III: 3rd International Conference on Refining of Iron and Steel by Powder Injection* (Lulea, Sweden: MEFOS, 1983).
54. O. Haida, T. Emi, S. Yamada, and F. Sudo, *Scaninject II: 2nd International Conference on Injection Metallurgy* (Lulea, Sweden: MEFOS, 1980).